CONF-830607--4

CONF-830607--4

DE83 009682

THEORY AND APPLICATION OF A THREE-DIMENSIONAL CODE SHAPS TO COMPLEX PIPING SYSTEMS

C. Y. Wang*
Reactor Analysis and Safety Division
Argonne National Laboratory
9700 South Cass Avenue
Argonne, IL 60439, U.S.A.

DISCLAIMER

*Member ASME

ABSTRACT

This paper describes the theory and application of a three-dimensional computer code SHAPS to the complex piping systems. The code utilizes a two-dimensional implicit Eulerian method for the hydrodynamic analysis together with a three-dimensional elastic-plastic finite-element program for the structural calculation. A three-dimensional pipe element with eight degrees of freedom is employed to account for the hoop, flexural, axial, and the torsional mode of the piping system.

In the SHAPS analysis the hydrodynamic equations are modified to include the global piping motion. Coupling between fluid and structure is achieved by enforcing the free-slip boundary conditions. Also, the response of the piping network generated by the seismic excitation can be included.

A thermal transient capability is also provided in SHAPS. An energy equation is used to compute the coolant temperatures due mainly to the heat convection. This equation is linked together with a radial heat-conduction equation to establish the temperature profile throughout the pipe-wall thickness. Thermal mechanical stresses are calculated by a thermo-viscoplasticity constitutive equation. The flow stress is then determined by an associated flow rule via Newton-Raphson procedure.

To illustrate the methodology, many sample problems dealing with the hydrodynamic, structural, and thermal analyses of reactor-piping systems are given. Validation of the SHAPS code with experimental data is also presented.

INTRODUCTION

During postulated accident events, the piping systems of nuclear reactors can be subjected to transient loadings of different types: (1) hydrodynamic loading resulting from pressure-wave propagation due to a core-disruptive accident (CDA) or a sodium-water reaction (SWR), (2) thermal loading generated by hot coolant sudden entering into the piping system, (3) structural loading due to seismic events, and (4) existent loads in the piping system engendered by normal reactor operation, such as internal pressurization, thermal effects, and creep phenomena. Because of geometry complexity and different types of loadings involved in the piping system, development of the multi-dimensional techniques or computer programs to assess the piping integrity is essentially a necessity.

Some of the postulated accidents for Liquid Metal Fast Breeder Reactors (LMFBR) can be analyzed as a piping system subject to simultaneous pressure pulses of high magnitudes. Examples of such accidents are a CDA for the primary heat transport systems and SWR for the secondary heat transport systems. The analysis of the interactions of the applied pressure pulses with one another and with the different components of the piping system can become extremely complex depending on the layout of the system, the number of the applied pulses, and the number and types of the components in the piping system. For example, the degree of complexity generated by the pressure wave propagation during an CDA can be imaged from the typical piping loop of the primary heat-transport system shown in Fig. 1.

Fig.1 Typical primary heat-transport system of looped LMFBR

The structural response of a piping system to the applied and subsequently propagating pressure pulses can be visualized to consist of two distinct modes: the breathing mode of the structural components as a direct result of the internal pressure, and the flexural mode of the system as it moves in the three-dimensional space. The two modes can be adequately represented by a bi-axial state of stress. Such stress is usually generated from the combination of: (1) an axial stress resulting from the axial extension and contraction of the piping components, the flexural bending of the pipes and components in two orthogonal planes, and the axisymmetric bending of the pipe walls; (2) a hoop stress resulting from the pipe-wall radial expansion or contraction; and (3) a shear stress resulting primarily from the torsion of the pipes and components.

To perform the structural analysis of piping systems generated by various loadings mentioned early, a piping analysis program was initiated in the Reactor Analysis and Safety Division of Argonne National Laboratory. The ICEPEL code [1] was developed to perform a coupled hydrodynamic-structural analysis of piping systems in two dimensions. The ICEPEL code is an extension of the ICECO code [2] developed early for LMFBR containment analysis. In ICEPEL, the Implicit Continuous-Fluid Eulerian finite difference hydrodynamics [3] is coupled to a nonlinear elastic-plastic explicit finite-element model of the piping system using thin axisymmetric shell element and co-rotational coordinate formulation [4].

Although the ICEPEL code can treat complex wave propagation in the piping system in two dimensions, it considers only the breathing mode of the pipes and components by ignoring the globe motion of the piping system. Furthermore, the code requires the centerline of all pipes and components to be fixed in space and has no thermal-stress calculational capabilities.

To provide an integrated analysis of piping systems a three-dimensional

been developed. In the structural analysis, SHAPS utilizes a three-dimensional pipe element with eight degrees of freedom at each node, using co-rotational coordinates in the mathematical formulations [5]. Six degrees of freedom, three displacements and three rotations, describe the flexural motion in three-dimensional space. The remaining two degrees of freedom describe the axisymmetric breathing mode in terms of hoop displacement and wall bending rotation. In addition, a spring element is used to model piping supports, such as snubbers and hangers. Thus, the structural analysis considers hoop, flexural, axial, and torsion modes of the piping systems.

In this paper, the aspects of hydrodynamics and the coupling of the three-dimensional structural analysis to the two-dimensional Eulerian hydrodynamics are addressed, together with the description of the thermal transient capability developed recently. Sample problems are given regarding applications of the SHAPS code to the response of piping systems generated by various accident loads.

HYDRODYNAMICS

As the pipe system moves in a three-dimensional space, it carries along with it the flowing fluid. The hydrodynamic finite-difference mesh is also assumed to be carried along with the pipe system without changing its shape or its size. Nevertheless, the fluid remains free to slide along the pipe wall and the pipe remains free to twist independently of the fluid.

Such assumed motion of the finite-difference mesh is to be considered in the hydrodynamic governing equations in a global sense, assuming that the axisymmetry of the fluid flow is maintained, at least within each individual pipe element.

Generalizing the problem, let us consider a control volume V bounded by a surface S and moving with an arbitrary velocity $\bar{V}^G$. The conservation of mass and momentum of the fluid flowing through V can be written as

$$\int_V \frac{\partial \rho}{\partial t}\, dV + \int_S \rho \bar{V}_i^D \hat{n}_i\, dS = 0 , \tag{1}$$

and

$$\int_V \frac{\partial \rho \bar{V}_i}{\partial t}\, dV + \int_S \rho \bar{V}_i \bar{V}_j^D \hat{n}_j\, dS = \int_S -P \hat{n}_i\, dS , \tag{2}$$

where $\hat{n}$ is a unit vector normal to the control surface S, ρ is the density, P is the fluid pressure, $\bar{V}_i$ is the fluid velocity, and

$$\bar{V}^D = \bar{V} - \bar{V}^G . \tag{3}$$

In Eq. (2), the viscous and gravity terms are neglected for simplicity.

Furthermore, since the fluid and the finite-difference mesh are moving together in the transverse direction, one can easily see that such a motion is equivalent to a case in which the control volume is fixed in the radial direction, i.e., U^G (the radial velocity component of $\bar{V}^G$) is zero.

Therefore, in terms of the cylindrical velocity components u, in the radial direction, and v, in the axial direction, and considering the viscous forces in the momentum equations, Eqs. (1) and (2) can be written as

$$\frac{\partial \rho}{\partial t} + \frac{1}{r}\frac{\partial (r \rho u)}{\partial r} + \frac{\partial (\rho v^D)}{\partial z} = 0 , \tag{4}$$

$$\frac{\partial(\rho u)}{\partial t} + \frac{1}{r}\frac{\partial(\rho u^2 r)}{\partial r} + \frac{\partial(\rho u v^D)}{\partial z} = -\frac{\partial(p+q)}{\partial r} + \mu\frac{\partial}{\partial z}\left(\frac{\partial u}{\partial z} - \frac{\partial v}{\partial r}\right), \tag{5}$$

and

$$\frac{\partial(\rho v)}{\partial t} + \frac{1}{r}\frac{\partial(\rho u v r)}{\partial r} + \frac{\partial(\rho v^D v)}{\partial z} = -\frac{\partial(p+q)}{\partial z} - \frac{\mu}{r}\frac{\partial}{\partial r}\left(r\left(\frac{\partial u}{\partial z} - \frac{\partial v}{\partial r}\right)\right), \tag{6}$$

where v^D is defined by an equation similar to Eq. (3), and

$$q = -(\lambda + 2\mu)\left(\frac{1}{r}\frac{\partial(ur)}{\partial r} + \frac{\partial v}{\partial z}\right). \tag{7}$$

In the above equations λ and μ are the first and second coefficients of viscosity of the fluid, respectively.

The above governing equations are similar to the standard equations for the Implicit Continuous-fluid Eulerian (ICE) method [3] with only one exception, that v^D appears in some of the convective terms instead of the standard fluid velocity v. Following the ICE differencing scheme, which assigns the pressures and densities to the center of the zone and the velocity components to the center of the zone boundary normal to their direction, the differences between the above governing equations and the standard ICE equations [3] are reflected only in the source terms $R_{i+1/2,j}$ and $S_{i,j+1/2}$ of the ICE-difference momentum equations in $G_{i,j}$ of the ICE-Poisson equation.

FLUID-STRUCTURAL COUPLING

To account for the pipe-wall hoop motion in the hydrodynamics, we consider a free-slip fluid interface motion with respect to the pipe wall. The fluid interface motion is contemplated as equivalent to that of a free surface with an applied pressure distribution. Given the pipe-wall shell motion with respect to the pipe axis, as obtained from the structural computations, one can produce that same motion of the fluid interface with some unique pressure distribution applied to the interface.

The fluid interface with the pipe wall is defined by a locus of points representing the end points of the pipe shell for all structural pipe elements. Straight-line segments are assumed to join these points and thus define the shape of the interface. In general, the midpoints of each of these straight-line segments will not lie on any of the Eulerian mesh lines used in the finite-difference solution of the hydrodynamic equations. The finite-difference zones in which such points lie are flagged as boundary zones. The pressure at the center of these boundary zones determines the motion of the fluid interface with respect to the pipe axis. The pressures in the boundary zones are either adjusted iteratively or computed explicitly until the motion of the fluid interface conforms with the motion of the pipe wall, so that the fluid can freely slide along the tangent to the wall. In the direction normal to the wall, the fluid and the wall move together.

Implicit Method

The following relaxation equation is used to compute the pressure in the boundary zones [2]:

$$p^{k+1}_{i,j} = p^{k}_{i,j} - \frac{\Delta\tau}{\delta}\left(\vec{v}_p^{\,n+1}\right)^k - \vec{v}_b^{\,n+1} \cdot \hat{n}_{i,j}, \tag{8}$$

where $\hat{n}$ is a unit normal vector pointing to the fluid and defined at the midpoint of the straight-line segment associated with finite-difference boundary zone (i,j), $\vec{v}_b$ is the velocity vector of the midpoint of the wall segment associated with zone (i,j), $\vec{v}_p$ is the velocity vector of the fluid particle at the

midpoint of the wall segment, $\Delta\tau$ is a relaxation parameter, and δ is a zone-size parameter. Superscript k counts iterations, whereas n counts time steps. Clearly, $\hat{v}_p^{n+1}$ is one of the iterates and must be recomputed each time the pressure and velocities are adjusted.

Iterating Poisson's equation of the Implicit Continuous-fluid Eulerian (ICE) method for the interior zones and Eq. (8) for the boundary zones using the new iterates of pressures in zones (i-1,j) and (i,j-1), while sweeping the mesh in the direction of increasing i and j, is equivalent to a successive overrelaxation scheme. Von Newmann's Fourier stability analysis of the difference equations in such a scheme yields a relaxation parameter $\Delta\tau$:

$$\Delta\tau \leq \frac{\rho\delta^2}{2\Delta t} \quad . \tag{9}$$

The use of Eq. (8) and Eq. (9) shows that the pressures in the boundary zones are adjusted by an amount proportional to the fluid mass flow rate across the wall. The boundary-zone pressure is increased when the fluid is crossing the wall and is decreased when the fluid is pulling away from the wall.

To evaluate the bracketed term of Eq. (8), we refer to Fig. 2 which shows the pipe-wall segment (fluid interface) of pipe element k in relation to the Eulerian finite-difference mesh. The boundary zone is flagged with the letter B in the upper left corner. The midpoint of the wall segment is b, and the fluid particle next to it is p.

Fig.2 Effect of pipe-wall hoop motion on hydrodynamics

The Eulerian finite-difference mesh is assumed to be fixed to the co-rotational coordinate system of the element. Hence, the fluid velocities, which are computed with respect to the Eulerian mesh, are velocities as seen from the co-rotational coordinate system of the element. Furthermore, the pipe-shell hoop motion due to internal pressurization is also referred to the co-rotational coordinates of the element. Therefore, the fluid-velocity components of the particle p relative to the pipe wall are $u_p - u_b$ in the radial direction and v_p

in the axial direction. Thus, the fluid velocity relative to the pipe wall and along the vector n is $v_p \sin\theta - (u_p - u_b)\cos\theta$.

Explicit Method

At the beginning of a hydrodynamic computational cycle, the structural results using the pressure of the previous hydrodynamic cycle are readily available. From such results, the velocity of the structure at the midsegment point b is available. For example, the radial velocity at b is

$$u_b = 0.5(\dot{w}_N + \dot{w}_{N+1}) \quad . \tag{10}$$

Next, the hydrodynamic pressures in all fluid zones are computed using Poisson's equation, and the fluid velocities at the boundaries between any two fluid zones are computed using the momentum equations. Since the fluid is assumed to slip freely along the pipe walls, the axial velocities in the boundary zone are set equal to the axial velocity in the zone across the wall. The axial velocity at p is then evaluated by linear interpolation among the nearest axial velocity stations.

Now, the radial velocity component at p is set to satisfy the condition that the fluid particle p and the midsegment point b move together in a direction normal to the wall. Thus,

$$u_p = u_b + (v_p - v_b)\tan\theta \quad . \tag{11}$$

Using u_p, $u_{i-(1/2),j}$, and the known position of p, we compute the radial velocity $u_{i+(1/2),j}$ by linear interpolation between u_p and $u_{i-(1/2),j}$; thus,

$$u_{i+(1/2),j} = \frac{\Delta R}{\Delta R + S} u_p + \frac{S}{\Delta R + S} u_{i-(1/2),j} \quad . \tag{12}$$

Finally, the radial momentum equation is used to compute the pressure in the boundary zone $P_{i+1,j}$, knowing $u_{i+(1/2),j}$; thus,

$$P^{n+1}_{i+1,j} = \frac{\Delta R}{\phi}\frac{\phi}{\Delta R} P^{n+1}_{i,j} + \frac{1-\phi}{\Delta R} P^{n}_{i,j} - P^{n}_{i+1,j} + R_{i+(1/2),j} + \frac{(\rho u)^{n}_{i+(1/2),j} - (\rho u)^{n+1}_{i+(1/2),j}}{\Delta t} \quad . \tag{13}$$

THERMAL ANALYSIS

Energy Equation

One capability has been introduced in the SHAPS code pertains to the treatment of the thermal shock that could be experienced by the primary piping system due to either cooling fluctuations in the core or the pre-existing thermal gradient during the normal operating condition. Here an energy equation is developed that provides temperature distribution in the piping system.

In the differential form, the energy equation derived from the piping configuration and the corresponding control volume shown in Fig. 3 is

$$\bar{\rho}c\frac{\partial T}{\partial t} = k\frac{\partial^2 T}{\partial z^2} - \bar{\rho}\bar{v}\bar{c}\frac{\partial T}{\partial z} - \bar{p} + 1/2\,\bar{\rho}\bar{v}^2 - (\lambda + 2\mu)\frac{\partial v}{\partial z}\frac{\partial \bar{v}}{\partial z} + \frac{2}{R} h_i (T_1^W - T) - P_B u^W \quad , \tag{14}$$

where $\bar{\rho}$ is the average density at a cross section perpendicular to the pipe line, c the specific heat constant, T the temperature, v the average axial fluid velocity, p the average pressure, λ and μ the viscosity coefficients, R the pipe inner radius, h_i the coefficient of heat transfer at the inside surface of the wall, T_1^W the wall temperature at the inner surface, P_B the pressure at the pipe boundary, and u^W the wall radial velocity.

The energy equation can be further written into the finite-difference form (see Fig. 3) which yields

$$c\bar{\rho}_{i,j} \frac{T_j^{n+1}}{\delta t} = c\bar{\rho}_{i,j} \frac{T_j^n}{\delta t} + \frac{k}{\delta z^2} (T_{j+1} + T_{j-1} - 2T_j)$$

$$+ c(\bar{\rho}\bar{v})_{i,j} \frac{T_{j-1} - T_{j+1}}{2\delta z} + (\bar{p} + 1/2\ \bar{\rho}\bar{v}^2)_{i,j} \left(\frac{\bar{v}_{i,j-1/2} - \bar{v}_{i,j+1/2}}{\delta z}\right)$$

$$+ (\lambda + 2\mu)\ (\bar{v}_{i,j-1/2} - \bar{v}_{i,j+1/2})/\delta z + \frac{2}{R_i}\ h_i\ (T_1^W - T_j)$$

$$- p_j^B\ u_j^W \quad . \tag{15}$$

Fig.3 Control volume for derivation of energy equation

Heat-Conduction Equation

The heat conduction model of the SHAPS code utilizes a one-dimensional radial heat conduction equation to determine the temperature profile through the wall. This equation is

$$\rho_w\ c_w \frac{\partial T^W}{\partial t} = \frac{1}{r} \frac{\partial}{\partial r} \left(k_w r \frac{\partial T^W}{\partial r}\right) \quad , \tag{16}$$

where ρ_w is the density of the pipe wall; c_w is the heat capability of the wall material; k_w is the heat-conduction coefficient of the solid wall; T^w is the wall temperature; and r is the radial position of the temperature zone. Note that for isotropic homogeneous materials, the thermal conductivity k_w can be factored out of the right-hand side of Eq. (16).

To obtain the temperature distribution throughout the pipe wall, Eq. (16) is written implicitly into finite-difference form with respect to the control volume shown in Fig. 4. The resulting finite-difference heat conduction equation is

$$\frac{T_j^{n+1} - T_j^n}{\delta t} = \frac{\alpha}{r_j \, \delta r_w^2} \, T_{j+1}^{n+1} \left(r_j + \frac{\delta r_w}{2}\right) + T_{j-1}^{n+1} \left(r_j - \frac{\delta r_w}{2}\right) - 2r_j \, T_j^{n+1} \quad , \quad (17)$$

where

$$\alpha = \frac{k_w}{\rho_w \, c_w} \quad .$$

Note that the finite-difference heat conduction equation applies only to the interior temperature nodes. In other words, for the finite difference temperature mesh shown in Fig. 11, Eq. (17) valids for j = 2, 3, . . . , J-1.

Fig.4 Control volume for derivation of the finite-difference heat-conduction equation

At the inner and outer surfaces of the pipe wall the temperature boundary conditions must be satisfied. Thus, at the inner surface where the hot coolant contacts with the pipe wall the convective boundary condition is

$$h_i \, (T_f - T_1^{n+1}) = - \, k_w \, \frac{\partial T}{\partial r} \Big|_1^{n+1} = \frac{k_w}{2\delta r_w} \, (T_0^{n+1} - T_2^{n+1}) \quad , \quad (18)$$

where understandably T_f is the fluid temperature; T_1 is the wall temperature at the first node; h_i is the heat transfer coefficient; and T_0 and T_2 are temperatures at nodes 0 and 2, respectively.

The heat transfer coefficient h_i is determined from the characteristic of the fluid. Presently, two formulas are available: one for liquid metals and one for other regular fluids. Prandtl's number is the criteria that determines which formula is to be used. Denoting Reynold's number and Prandtl's number by R_e and P_r, respectively, the heat transfer coefficient for liquid metals has the form

$$h_i = k_f \left[5 + 0.025 \left(R_e P_r\right)^{0.8} \right] / 2R_i \quad .$$

For other fluids the coefficient h_i is

$$h_i = k_f \left[0.023 \, R_e^{0.8} \, P_r^{0.333} \right] / 2R_i \quad .$$

On applying Eq. (16) at node 1 and eliminating T_0^{n+1} we obtain

$$T_1^{n+1} \left[1 + a + ab_i \right] - aT_2^{n+1} = T_1^n + ab_i \, T_f \quad , \tag{19}$$

where

$$b_i = \frac{\delta r_w \, h_i}{k_w} \left(1 - \frac{\delta r_w}{2R_i}\right) \quad .$$

Similarly, at the outer surface (node J) of the pipe wall the temperature equation is

$$T_j^{n+1} \left[1 + a + ab_o \right] - aT_{j-1}^{n+1} = T_j^n + ab_o \, T_\infty \quad , \tag{20}$$

where

$$b_o = \frac{\delta r_w \, h_o}{k_w} \left(1 + \frac{\delta r_w}{2R_o}\right) \quad ,$$

h_o is the heat transfer coefficient of the material outside the pipe; R_o is the pipe outer radius; and T_∞ is the ambient temperature.

Combining Eqs. (17), (19), and (20) the temperature at each node can be solved by the regular iteration method.

Thermo-Viscoplasticity Constitutive Equations

The mathematical model for the thermal-stress analysis is applicable to the behavior of a large number of materials under a variety of loading conditions, such as thermal, plastic, and viscous effects. This model is termed as "thermo-viscoplastic" even though elastic behavior is also included.

For many materials the simplifying assumptions of isotropy and a Von Mises flow criterion are justified by experimental data. Thus, for the problem involving calculations of thermal-mechanical stress the basis of the approach is to solve the flow condition [6]

$$\phi = \bar{\sigma} - H \left(\bar{\varepsilon}^i, \dot{\bar{\varepsilon}}^i, T \right) \quad , \tag{21}$$

in which $\bar{\sigma}$ and H denote the effective stress and flow stress, respectively; $\bar{\varepsilon}^i$ and $\dot{\bar{\varepsilon}}^i$ are the effective inelastic strain and its rate; and T is the temperature.

SAMPLE PROBLEMS

Experimental Validation of Fluid-Structure Interaction

Test FP-E-103 of a single elbow piping system is one of the simple elastic-plastic piping experiments performed by SRI International [7] for verifying

piping codes, such as ICEPEL [8] and PTA-2 [9]. The same test is analyzed here using the new three-dimensional coupled code SHAPS. The purpose of this analysis is (1) to validate the fluid-structure interaction scheme, (2) to investigate the flexural response of a single elbow configuration to internally propagating pressure pulses, and (3) to estimate the pressure attenuation along the elbow. Since the entire results are quite voluminous only important portions are presented here.

A schematic of the experimental layout and the instrumentation locations of test FP-E-103 are shown in Fig. 5. A specially designed and calibrated pulse gun is directly flanged to a thick-walled stainless steel pipe of 8.26 cm (3.25 in) outside diameter, 0.48 cm (0.188 in) wall thickness, and 304.8 cm (10 ft) length. This pipe is directly flanged to a thin-walled Nickel-200 test pipe which is 152.4 cm (5 ft) long and has an outside diameter of 7.62 cm (3 in) and a wall thickness of 0.165 cm (0.065 in). The thin-walled test pipe is connected in series to identical pipe through a 90° thick-walled stainless steel elbow of 11.43 cm (4.5 in) radius of curvature and 0.762 (0.3 in) wall thickness. The second flexible pipe ended with a heavy blind flange.

Fig.5 Layout of the SRI Pipe-Elbow Experiment

A typical comparison between the calculated pressure history and the measured one at gage P2 inside the thick-walled pipe is shown in Fig. 6. Considering the effects of implicit hydrodynamic computations in smearing off sharp pressure peaks, the agreement between the calculations and the experimental results in pulse shape, time of arrival and magnitude is excellent. Cavitation, which is indicated in the measurements of the zero pressure, is well predicted by the calculations which uses a zero cut-off pressure. At gages P4 and P5 a very good agreement in all aspects of the incident pressure pulse is found from comparisons between the calculated and the measured pressure histories. The plastic deformation of the pipe walls caused a significant reduction in the pressure peak magnitude as the pulse propagates along the pipe. Dispersion of the pulse is also indicated in the wider pulse at P5 predicted by SHAPS.

Fig.6 Comparison of the calculated and measured pressure-time histories at gage P2 of the thick-wall stainless steel pipe

In the vicinity of the elbow, the comparisons between the calculated and the measured pressure histories for gages P8-P10 upstream from the elbow and gages P14-P16 downstream from it are shown in Figs. 7 and 8. In addition to the good agreement, it should be mentioned that the calculated peak pressure downstream from the elbow is about 3.35 MPa, which is slightly less than the calculated peak upstream from the elbow of about 3.61 MPa. A drop of about 7% as compared to the measured drop of about 18%.

Fig.7 Comparison of the calculated and measured pressure-time histories at gages P8-P10 of the first flexible pipe

Fig.8 Comparison of the calculated and measured pressure-time histories at gages P14-P16 of the second flexible pipe

It should also be noted here that the two-dimensional ICEPEL computations which ignore the flexural motion and treat the elbow wall as rigid had showed: (a) no drop in the peak pressure along the elbow and (b) slightly higher pressure levels - of about 4 MPa - in the flexible pipes as well as in the elbow. Similar results were obtained from the three-dimensional SHAPS computations when the flexural motion of the elbow nodes were constrained. Therefore, it is concluded that the calculated drop in peak pressure is due to the flexural motion of the elbow in response to the propagating pulse.

To illustrate the code capability on computing the circumferential strain the predicted and measured strains at gages SG11-SG15 located 7.62 cm (3 in) upstream from the elbow are given in Fig. 9. As can be seen that the calculated strains are well within the wide range of experimental strain measurements around the circumference of the pipe. The flexural displacements of the nodes along the piping system indicated that bending of the pipe occurred as a result of the propagation of pressure pulse around the elbow. Examination of the flexural displacements of the end of the calculation time indicates that, near the elbow, the pipe nodes moved transversely in the positive y-direction; while near the junction with the thick-walled pipe, the nodes moved transversely in the negative global y-direction. This configuration resembles the second bending mode. Such bending occurred inspite of the fact that the calculations started from a perfect pipe. Imperfections in commercial pipes are expected to enhance the bending response.

Fig.9 Comparison of the calculated and measured strain-time histories at gages SG_{11}-SG_{15} of the first flexible pipe

Therefore, it can be concluded that the wide variation in the circumferential strains around the circumference of the pipe is partly due to bending and partly due to variation in the wall thickness around the circumference.

Structural Response Analysis of the Steam Generator Piping System

The capabilities of the SHAPS code are further demonstrated from the analysis of a stream-generator piping loop shown in Fig. 10. This piping system consists of 8 straight pipes, 6 elbows, 1 reducer, 24 snubbers, and 5 hangers. Structurally, the system is represented by 91 pipe elements, 24 linear spring elements, and 116 nodes. Node 1 is at the inside end of the super heater outlet nozzle. Node 92 is at the inside end of the evaporator inlet nozzle. Other modelling features are listed as follows:

(a) Each elbow is represented by 3 straight pipe elements.

(b) The reducer is modeled by a sudden change in cross-sectional area at node 88.

(c) All snubbers are to be represented by linear spring elements without gaps (free play).

(d) The analysis is to be limited to elastic response using the linear elastic material properties of the 2 1/4 CR-1 Mo steel piping as given in Nuclear Systems Material Handbook.

(e) The input pressure pulse is to be simplified to a triangular pulse with a linear up ramp from zero to 1500 psi in 8.2 ms followed by a down ramp to zero pressure in 51.2 ms.

(f) A nonreflecting boundary is used at the superheater outlet nozzle.

(g) Structural nodes 1-5 and 90-92 are fixed in space as they represent the overstrong superheater-outlet and evaporator-inlet nozzles, respectively;

(h) nodes 93-116 representing the anchor points of the snubbers are also fixed in space.

Using the model described above three cases were considered by the SHAPS code:

Case 1, to represent the hangers as rigid by fixing the nodal displacement in the Y-direction at nodes 7, 25, 40, 59, and 86 (Fig. 28).

Case 2, to ignore the hangers by freeing the nodal displacement in the Y-direction at nodes 7, 25, 40, 59, and 86.

Case 3, similar to Case 2 but without the inline snubbers (S-44, 42, 34, 36, 30, 28, 18, 16, 14, 12, 10, and 8). A small stiffness of 10 lb/in is selected for these snubbers.

A study of the calculated pressure histories along the piping loop indicates that the change of both pressure peaks and pulse durations is small. This is because the piping system is responding elastically, and hence, the anticipated attenuation of pressure pulse peaks due to plastic deformation is eliminated. The results also show clear evidence of pressure pulse reflections along the system. These reflections are attributed to the reducer at node 88, the elbows, and the flexural response of the piping system.

To illustrate the 3-D response of the piping loop Figs. 11 and 12 compare the flexural displacements at nodes 37 and 64 for cases 1 through 3. From these figures one can see that: (a) the elimination of the rigid hangers has effected the amplitudes of displacements particularly in the Y-direction. The amplitudes are in general higher in the more flexible system of case 2. The frequency is slightly higher in the stiffer system of case 1. (b) The elimination of the inline snubbers in case 3 resulted bigger amplitudes and even lower frequencies than cases 1 and 2 as the system in case 3 is the most flexible.

Furthermore, examination of the stresses throughout the system indicated that the hoop stresses resulting from the internal pressurization are of the same order of magnitude as the axial stresses resulting from the bending of the pipes and of the walls. Therefore, consideration of hoop stresses, which are commonly ignored by general-purpose structural codes, are important in assessing the structural adequacy of piping systems.

Thermal Transient in a Straight Pipe

To illustrate the coupled hydrodynamic-thermal analysis, the SHAPS code was applied to the wave propagation in a water-filled straight pipe. Figure 13 shows the mathematical model used in the analysis in which a pipe of 1219.2 cm long was represented by 20 axial zones. A constant pressure of 50 Mpa and a

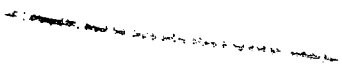

Fig.10 SHAPS model of the superheater to evaporator piping system

Fig.11 Flexural displacements as a function of time at node 27

Fig.12 Flexural displacements as a function of time at node 64

Fig.13 Mathematical model used in the SHAPS analysis

constant coolant temperature of 300°C are applied to the front junction of the pipe. The other end of the pipe is assumed to be a free surface. The ambient temperature of the coolant in the pipe is 30°C.

The pressure-time history at zone (2,9) is given in Fig. 14. Since the pressure pulse propagates with the speed of sound, disturbance arrives there at a very short time. Also, the effect of the free-surface rarefaction wave is clearly seen. Figures 15 and 16 depict the time histories of the fluid axial velocity and the coolant temperature at the same location. Because the thermal wave propagates with the fluid velocity it takes about 300 ms for the hot coolant to convect to the zone (2,9) and to reach the steady state temperature of 300°C. Results of this study indicate that propagation of the thermal wave is a slow process. The computed pressure of the fluid axial velocity and the coolant temperature at the same location. Because the thermal wave propagates with the fluid velocity it takes about 300 ms for the hot coolant to convect to the zone (2,9) and to reach the steady state temperature of 300°C. Results of this study indicate that propagation of the thermal wave is a slow process. The computed pressure and temperature histories provide useful information for calculating the thermal transient of the piping system.

CONCLUSION

A new three-dimensional code, SHAPS, for hydrodynamic, structural, and thermal analyses of piping systems has been developed. Presently, the code uses the implicit time integration scheme for both hydrodynamic and thermal transient analyses, together with an explicit time integration scheme for the structural calculation. It has been applied to a simple elastic-plastic single elbow piping experiment. The calculations compared favorably with the experimental measurements. Also, the calculations showed that an attenuation in peak pressure along the elbow occurs. Moreover, the SHAPS code is quite efficient. The CPU time for simulating this experiment is about 20 min on an IBM 370/195. This pressure attenuation results from the motion of the elbow. The good agreement achieved demonstrates that the SHAPS code is an accurate and useful tool for the LMFBR safety analysis.

Many areas of the SHAPS code still need additional research effort or improvement. First, as mentioned above, the code uses an explicit time integration scheme for the structural analysis. For dynamic problems that involve short solution times and high-intensity pressure loadings, explicit structural analysis is very efficient. However, for static or quasi-dynamic problems dealing with long-term calculations and slow-varying pressure loadings, such as those generated by thermal wave propagation, creep phenomenon or, normal operation pressurization, the explicit structural analysis could become very expesnive because of its restricted small time steps. Therefore, it is highly desirable to provide an option of using the implicit time integration scheme for the structural analysis so that problems involving long duration can also be analyzed.

Second, the structural program should be expanded by adding taper and curved pipe elements to model, respectively, the gradual flow-area change, as well as the increased flexibility of the elbow.

With the analytical development to be made in a continuous and progressive manner, the SHAPS code promises to be a significant step toward obtaining a better structural-hydrodynamic-thermal analysis of complex piping systems under transient condition. Piping support motion and external loadings, as well as thermal transients, can be considered in addition to the loading from internally propagating pressure pulses.

Fig.14 Pressure-time history at zone (2,9)

Fig.15 Fluid axial velocity as a function of time at zone (2,9)

Fig.16 Coolant temperature as a function of time at zone (2,9)

REFERENCES

1. A-Moneim, M. T., "Coupled Hydrodynamic-Structural Response Analysis of Piping System," ANL-77-91 (February, 1977).

2. Wang, C. Y., "ICECO - An Implicit Eulerian Method for Calculating Fluid Transient in Fast Reactor Containment," ANL-75-81 (December, 1975).

3. Harlow, F. H. and Amsden, A. A., "A Numerical Fluid Dynamics Calculation Method for All Flow Speeds," Journal of Computational Physics, Vol. 8, p. 197 (1971).

4. Belytschko, T. B. and Hsieh, B. J., "Nonlinear Transient Analysis of Shells and Solids of Revolution by Convected Elements," AIAA, Vol. 12, No. 8, p. 1031 (1974).

5. A-Moneim, M. T., Chang, Y. W., and Belytschko, T. B., "Three-dimensional Response of Piping Systems to Internally Propagating Pressure Pulses," Trans. 5th Intl. Conf. on Structural Mechanics in Reactor Technology, Paper E 3/3, Vol. E, Berlin, Germany (August, 1979).

6. Schreyer, H. L., Private Communication (July, 1980).

7. Cagliostro, D. J. and Romander, C. M., "Experiments on the Response of Flexible Piping Systems to Internal Pressure Pulses," SRI Fourth Interim Report on Project PYD-1960, SRI International, Menlo Park, CA (April, 1976).

8. A-Moneim, M. T. and Chang, Y. W., "Comparison of ICEPEL Predictions with Single-Elbow Flexible Piping Experiment," ASME Journal of Pressure Vessel Technology, Vol. 101, No. 2, pp. 142-148 (May, 1979).

9. Youngdahl, C. K., Kot, C. A., and Valentin, R. A., "Pressure Transient Analysis of Elbow-Pipe Experiments Using the PTA-2 Computer Code," ASME Journal of Pressure Vessel Technology, Vol. 103, No. 1, pp. 142-148 (February, 1981).

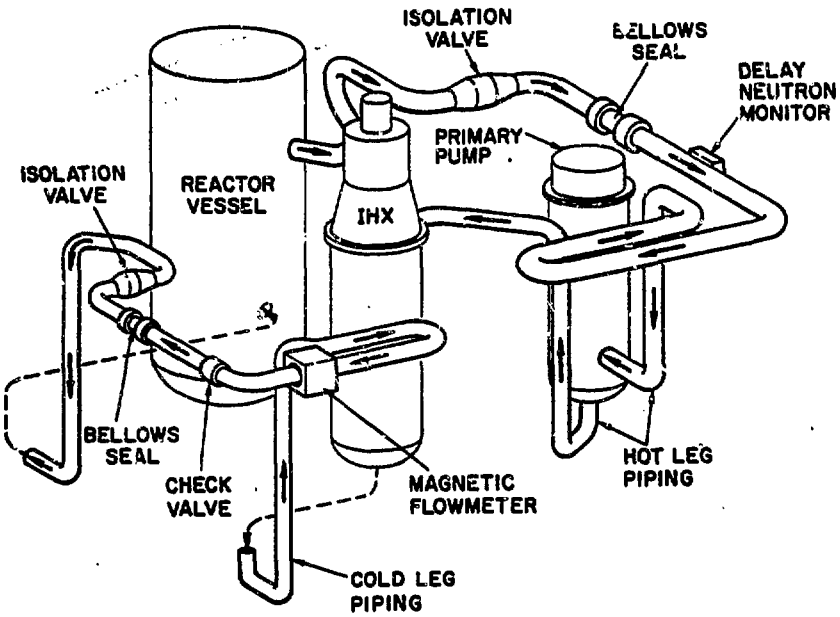
ISOLATION VALVE
BELLOWS SEAL
DELAY NEUTRON MONITOR
PRIMARY PUMP
ISOLATION VALVE
REACTOR VESSEL
IHX
BELLOWS SEAL
CHECK VALVE
MAGNETIC FLOWMETER
HOT LEG PIPING
COLD LEG PIPING

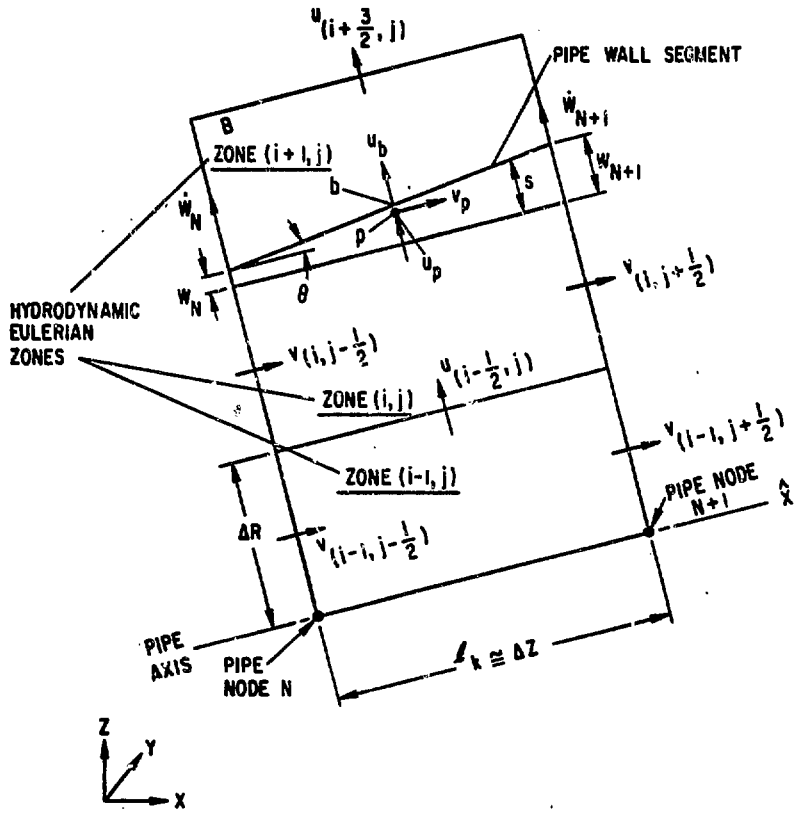
$u_{(i+\frac{3}{2},j)}$
PIPE WALL SEGMENT
B
ZONE (i+1, j)
u_b
b
v_p
s
$\dot{W}_{N+1}$
W_{N+1}
$\dot{W}_N$
p
u_p
W_N
θ
$v_{(i,j+\frac{1}{2})}$
HYDRODYNAMIC EULERIAN ZONES
$v_{(i,j-\frac{1}{2})}$
$u_{(i-\frac{1}{2},j)}$
ZONE (i, j)
$v_{(i-1,j+\frac{1}{2})}$
ZONE (i-1, j)
PIPE NODE N+1
ΔR
$v_{(i-1,j-\frac{1}{2})}$
PIPE AXIS
PIPE NODE N
$\ell_k \cong \Delta Z$
Z
Y
X

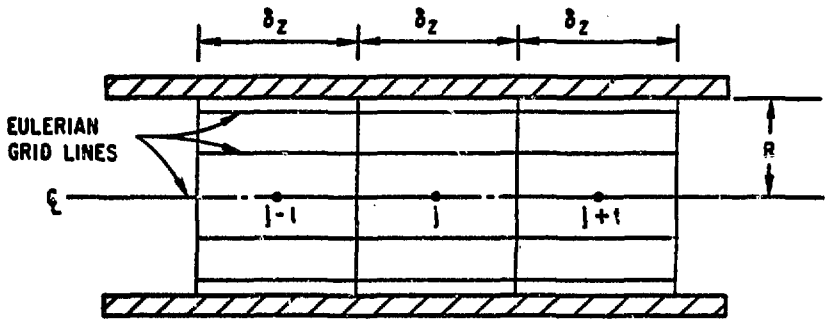

(a) MESH CONFIGURATION

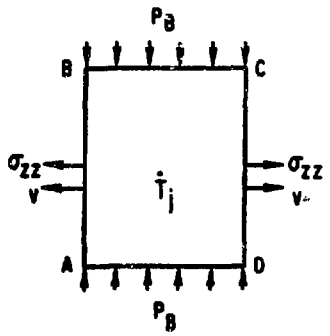

(b) CONTROL VOLUME

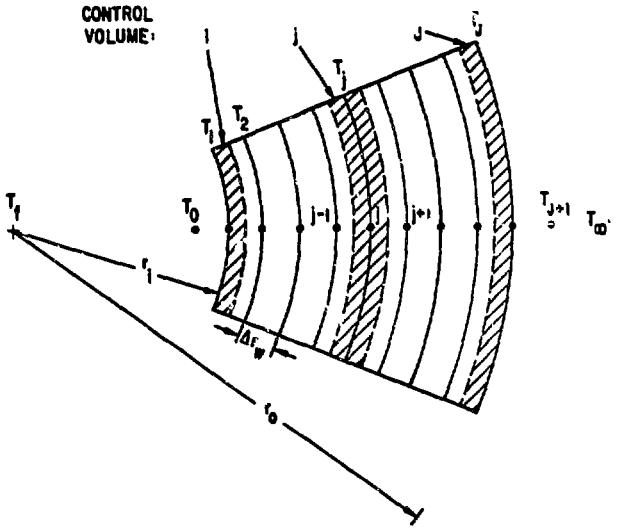
CONTROL VOLUME
1
j
J
T_J
T_j
T_1
T_2
T_f
T_0
j-1
j+1
T_{J+1}
T_∞
r_1
Δr_w
r_0

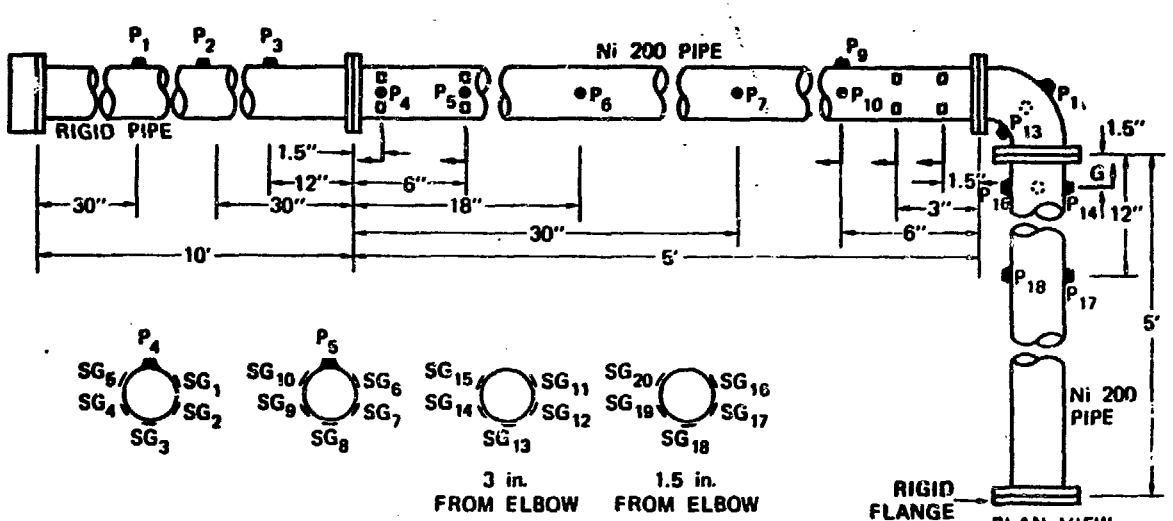
P1
P2
P3
P4
P5
P6
P7
P9
P10
P13
P14
P16
P17
P18
Ni 200 PIPE
RIGID PIPE
1.5"
12"
6"
30"
30"
18"
30"
10'
5'
1.5"
3"
6"
G
12"
5'
Ni 200 PIPE
RIGID FLANGE
PLAN VIEW
SG1
SG2
SG3
SG4
SG5
SG6
SG7
SG8
SG9
SG10
SG11
SG12
SG13
SG14
SG15
SG16
SG17
SG18
SG19
SG20
3 in. FROM ELBOW
1.5 in. FROM ELBOW
MA-1960-154b

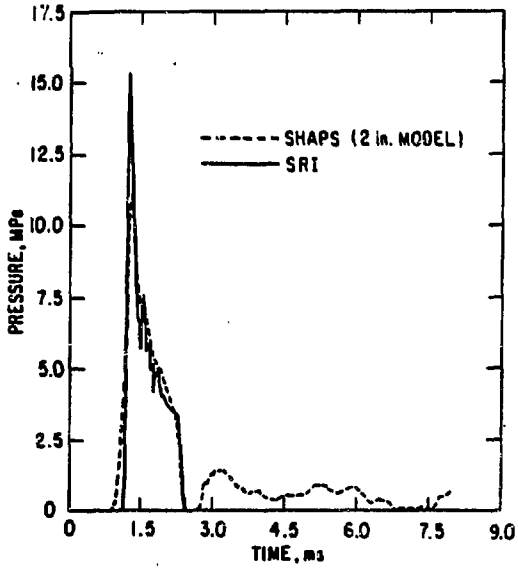
17.5
15.0
12.5
10.0
7.5
5.0
2.5
0
PRESSURE, MPa
SHAPS (2 in. MODEL)
SRI
0
1.5
3.0
4.5
6.0
7.5
9.0
TIME, ms

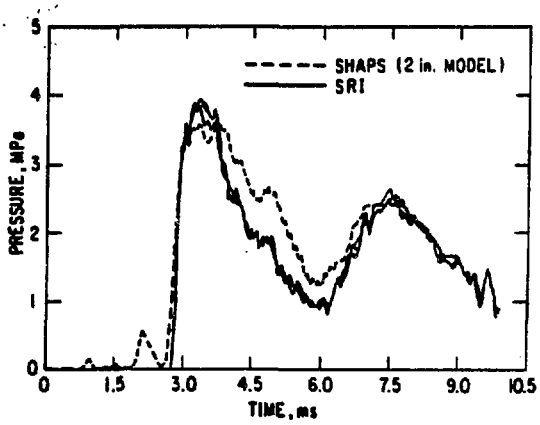
SHAPS (2 in. MODEL)
SRI
PRESSURE, MPa
TIME, ms
0
1
2
3
4
5
0
1.5
3.0
4.5
6.0
7.5
9.0
10.5

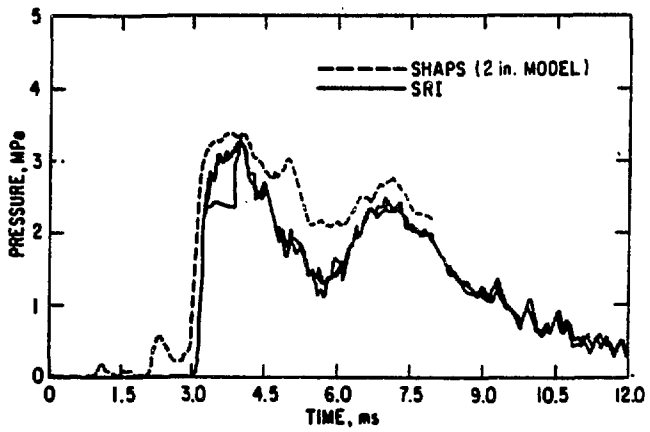
SHAPS (2 in. MODEL)
SRI
PRESSURE, MPa
TIME, ms
0
1
2
3
4
5
0
1.5
3.0
4.5
6.0
7.5
9.0
10.5
12.0

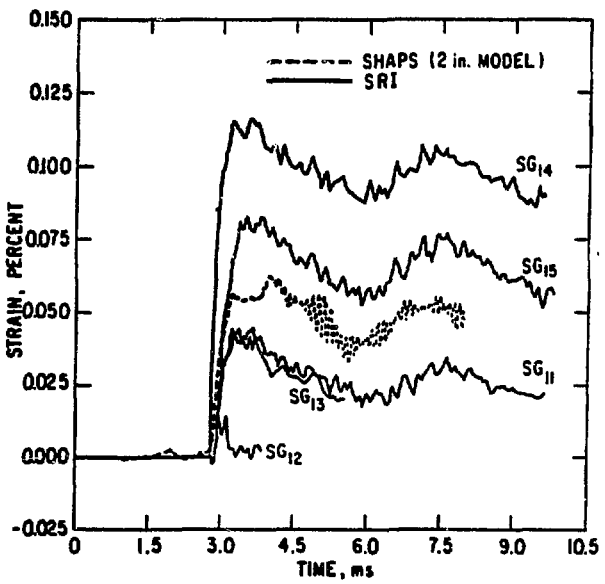
SHAPS (2 in. MODEL)
SRI
SG14
SG15
SG11
SG13
SG12
STRAIN, PERCENT
TIME, ms
0.150
0.125
0.100
0.075
0.050
0.025
0.000
-0.025
0
1.5
3.0
4.5
6.0
7.5
9.0
10.5

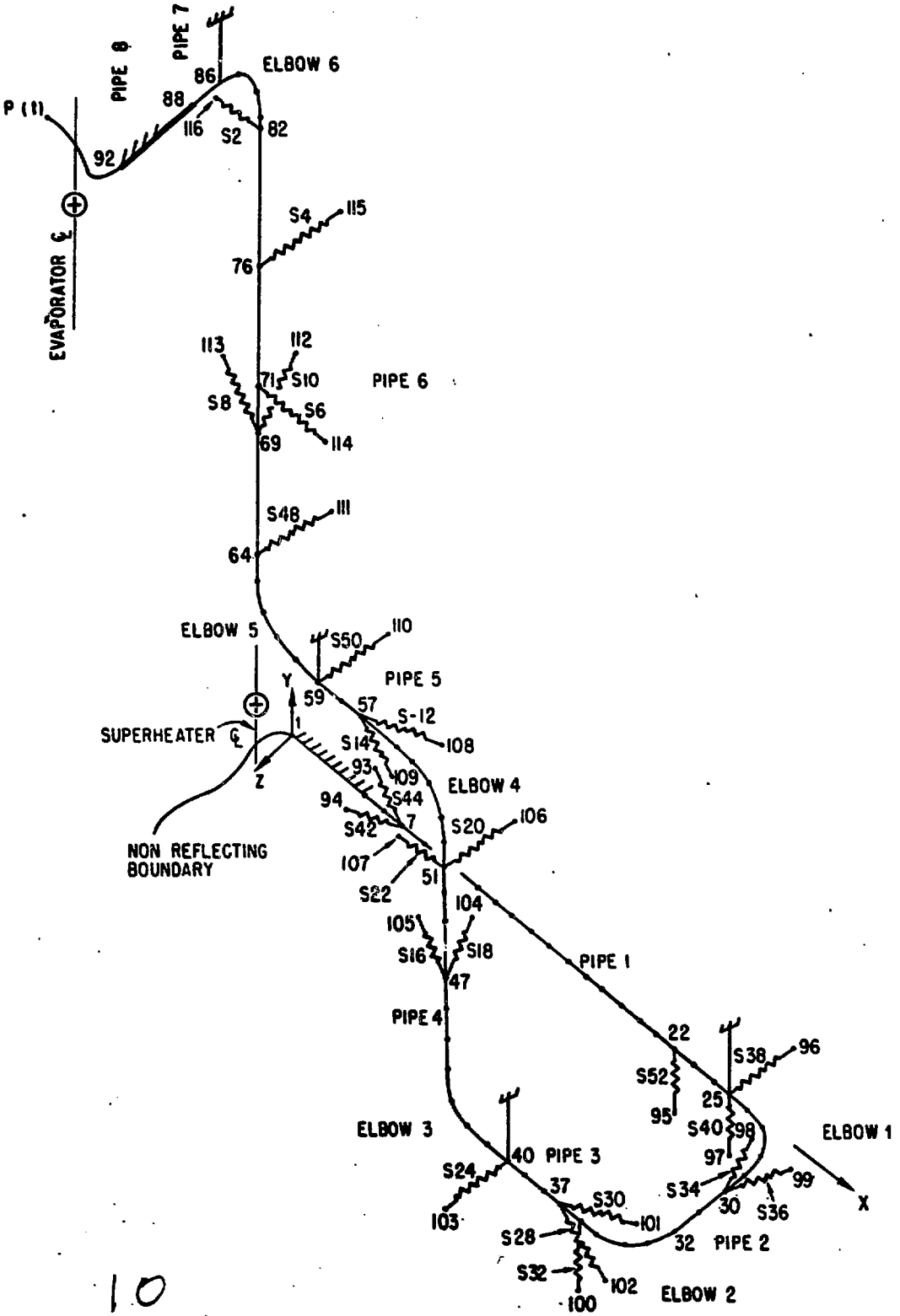
PIPE 8
PIPE 7
ELBOW 6
P (1)
86
88
116
S2
82
92
EVAPORATOR ℄
S4
115
76
113
112
71
S10
PIPE 6
S8
S6
69
114
S48
111
64
ELBOW 5
S50
110
PIPE 5
Y
59
57
S-12
108
SUPERHEATER ℄
1
S14
93
109
ELBOW 4
94
S44
S42
7
S20
106
NON REFLECTING BOUNDARY
107
51
S22
104
105
S16
S18
47
PIPE 1
PIPE 4
22
S38
96
S52
25
95
S40
98
ELBOW 1
ELBOW 3
40
PIPE 3
97
S24
37
S34
99
S30
30
S36
X
103
101
S28
32
PIPE 2
S32
102
100
ELBOW 2

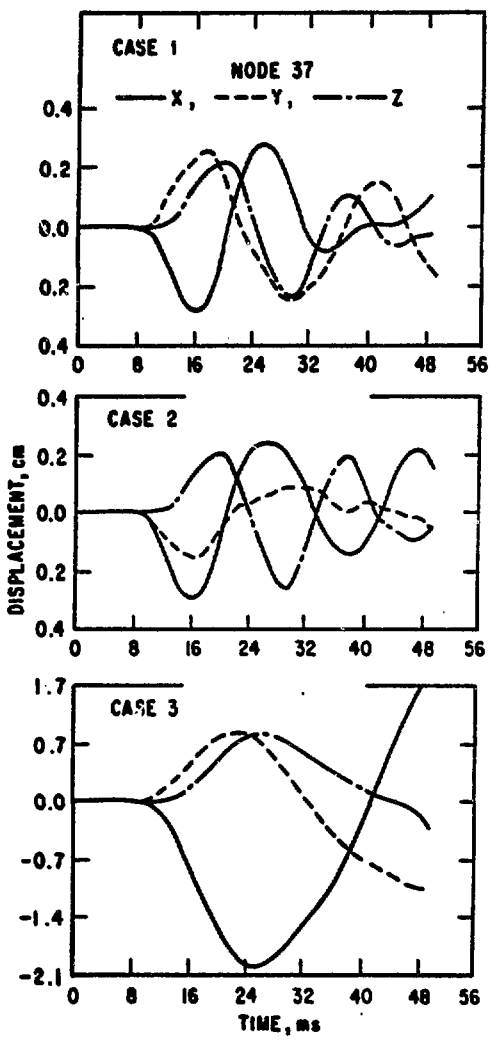
CASE 1
NODE 37
X, Y, Z
CASE 2
CASE 3
DISPLACEMENT, cm
TIME, ms
0.4
0.2
0.0
0.2
0.4
0
8
16
24
32
40
48
56
1.7
0.7
0.0
-0.7
-1.4
-2.1

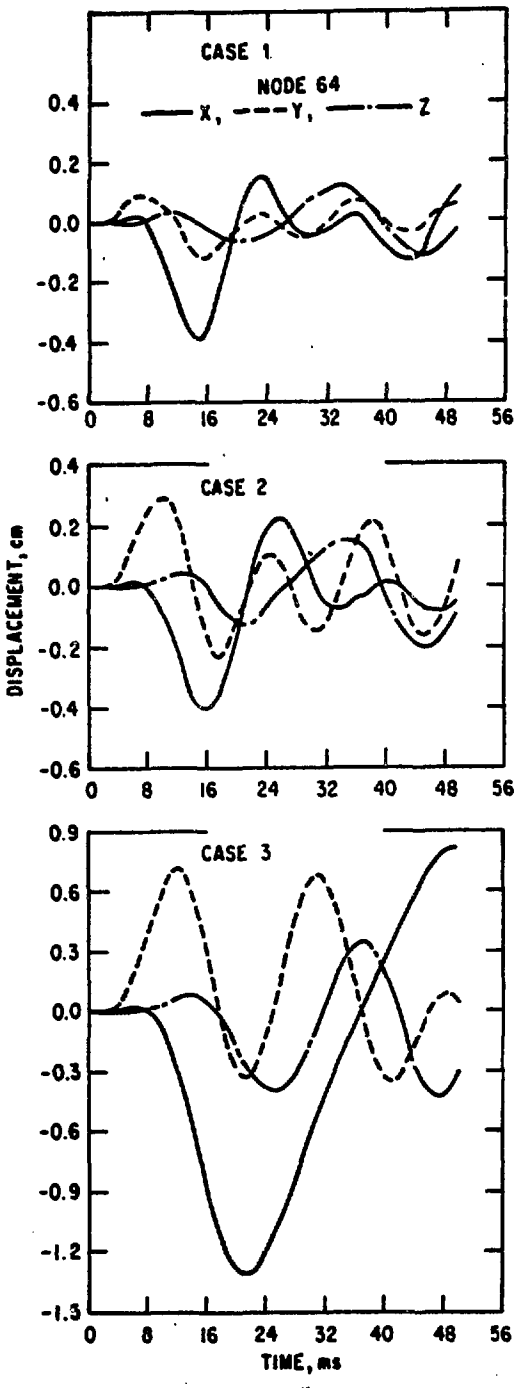
CASE 1
NODE 64
X, Y, Z
CASE 2
CASE 3
DISPLACEMENT, cm
TIME, ms

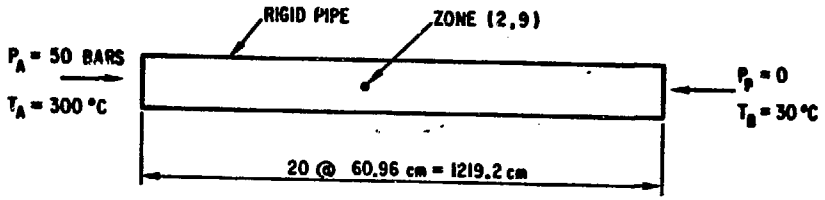
RIGID PIPE
ZONE (2,9)
P_A = 50 BARS
T_A = 300 °C
P_B = 0
T_B = 30 °C
20 @ 60.96 cm = 1219.2 cm

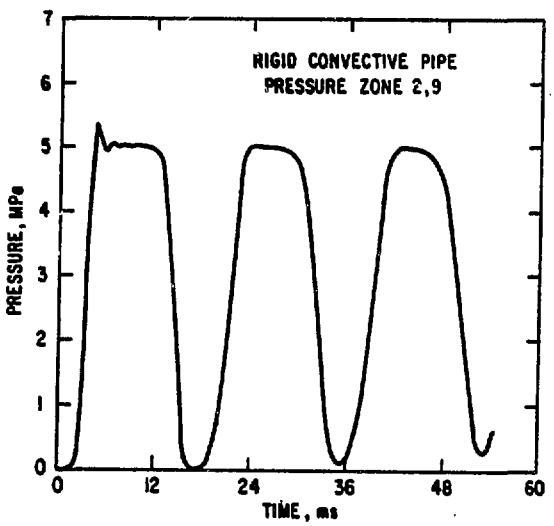
RIGID CONVECTIVE PIPE
PRESSURE ZONE 2,9
PRESSURE, MPa
TIME, ms
0
1
2
3
4
5
6
7
0
12
24
36
48
60

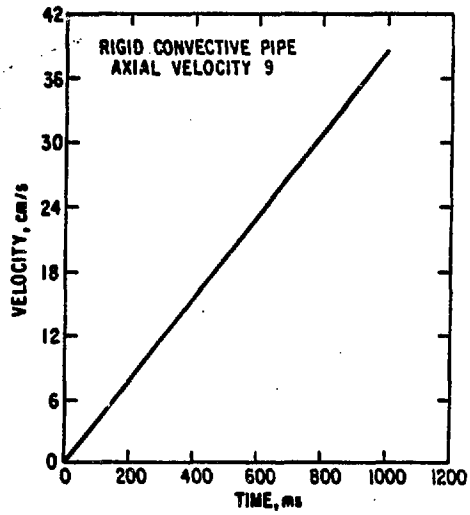
RIGID CONVECTIVE PIPE
AXIAL VELOCITY 9
VELOCITY, cm/s
TIME, ms
0
6
12
18
24
30
36
42
0
200
400
600
800
1000
1200

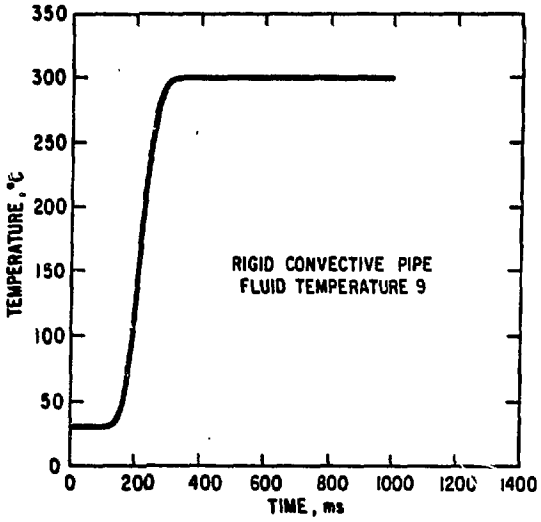
350
300
250
200
150
100
50
0
TEMPERATURE, °C
0
200
400
600
800
1000
1200
1400
TIME, ms
RIGID CONVECTIVE PIPE
FLUID TEMPERATURE 9